FULL PAPER

ROTI Keograms based on CMONOC to characterize the ionospheric irregularities in 2014

Jinghua Li[1*] , Guanyi Ma[1,2], Takashi Maruyama[1,3], Qingtao Wan[1], Jiangtao Fan[1], Jie Zhang[1] and Xiaolang Wang[1]

Abstract

Ionospheric irregularities have been studied since ~70 years ago. With the development of Global Navigation Satellite system (GNSS), networks of GNSS receivers have been used to obtain the characteristics of the irregularities, including the drift velocity, the structure, and the evolution. In this paper, keograms based on the Crustal Movement Observation Network of China (CMONOC) were used to characterize the irregularities over the area from longitude 85 to 125 °E and latitude 11 to 35 °N in 2014. Keograms were obtained for the rate of TEC index (ROTI) for every 0.5 degree longitude and 30 min universal time pixel. The results showed that the occurrence rate of irregularities in 2014 was high in the equinox months and December, and lowest in June. In equinox months the irregularities often appeared after sunset. In March the irregularities usually had long lifetime of ~5–7 h and ~5 degrees apparent longitudinal width. The long lifetime usually was accompanied by obvious eastward drift of ~100 m/s and large vertical ROTI (vROTI). In September the irregularities had weaker ROTI and shorter lifetime than those in March. The irregularities in the 2 equinox months should be related to the equatorial plasma bubbles (EPBs). In June, they appeared ~2–3 h later than those in equinoxes and drifted westward. The summer irregularities had weakest ROTI and their latitude was ~30 °N, much higher than those in equinoxes. In December, the irregularities were discrete patches with a longitudinal width of ~2 degrees and short lifetime of ~2 h. Unlike the equatorial irregularities in equinox months which are part of equatorial plasma bubbles, the solstice irregularities mainly appear to be a local phenomenon.

Keywords: ROTI, Ionospheric irregularity, Drift velocity, Keogram, Irregular patch

*Correspondence: jhli@nao.cas.cn

[1] National Astronomical Observatories Chinese Academy of Sciences, Beijing, China
Full list of author information is available at the end of the article

Li *et al. Earth, Planets and Space*   (2022) 74:149

Page 2 of 12

Graphical Abstract

ROTI Keograms based on CMONOC to characterize the ionospheric irregularities in 2014

vROTI keogram on March 1st 2014 based on CMONOC
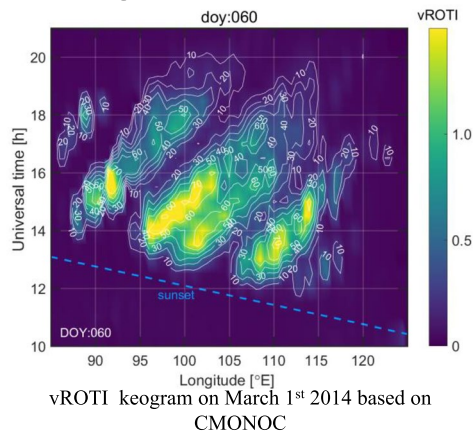
The vROTI keogram on March 1st 2014 showed that four main patches appeared at different longitudes. The apparent longitudinal width of each patch is ~5 degree, with a lifetime of 5~7 hours. The average velocity of each patch was estimated to be ~100m/s.

Using such keograms in 2014, the irregularities were analyzed over 85~125° E and 11~35° N. The patches on the keograms in equinox months were large with long lifetime and eastward drift. In the summer solstice month, the vROTI was weaker and the patches drifted westward. The patches in December were discrete and short lifetime. The irregularities in equinoxes may be related to the extension of the EPBs, and in the solstice months, they may be localized.

Introduction

Ionospheric equatorial plasma bubbles (EPBs) or irregularity is an important issue in space weather, because it can cause amplitude and phase fluctuation of radio signals passing through it, or even degrade the critical radio system performance. It has been widely studied by different techniques, such as ionosondes, radars, satellite in-situ measurement, airglow imagers, and the Global Navigation Satellite Systems (GNSS) receivers. Regarding the GNSS receivers, observation networks have been constructed, such as the International GNSS service (IGS), the GNSS Earth Observation Network System (GEONET) of Japan, the Crustal Movement Observation Network of China (CMONOC). Such networks make it possible to monitor the ionospheric parameters in a large area.

Two important parameters, total electron content (TEC) and rate of TEC index (ROTI), have been widely used to specify the ionosphere and ionospheric irregularities. TEC maps and ROTI maps are provided as products by some regional or global GNSS networks, such as IGS, GEONET and other organizations or institutes to present the background ionospheric condition and the occurrence of irregularities (Hernández-Pajares et al. 2009; Cherniak et al 2018). With an increasing number of receivers set up by CMONOC, TEC maps and ROTI maps based on CMONOC have been used to study the ionospheric irregularities over China and adjacent regions (Aa et al. 2018; Wei et al. 2020).

Although successive ROTI maps can show the temporal–spatial evolution of the ionospheric irregularities, they cannot succinctly summarize the continuous monitoring and the kinematic movement of the irregularities. Based on the high-density GPS observations over Southeast Asia, ROTI keogram was used to study the irregularities (Buhari et al. 2014). ROTI keogram is a cross section of ROTI at various times and longitudes or latitudes. The onset time, onset location, zonal width, lifetime, propagation distance, and average velocity of EPBs can be obtained from the ROTI keogram (Buhari et al. 2014). Buhari et al. (2014) also compared the results from ROTI keograms with the 630 nm airglow imager, and proved the coexistence of airglow depletions and ROTI enhancements (Buhari et al. 2014). TEC keogram was also used to study the ionospheric irregularities over South America section by Diego Barros et al. (2018) and de Jesus et al. (2020). Their results suggest that TEC/ROTI keogram offers a powerful tool for continuous monitoring and studying of large-scale plasma irregularities.

In this study a longitude-time vertical ROTI (vROTI) keogram based on CMONOC is obtained to show the characteristics of the irregularities. A large coverage of the area allowed us to monitor several irregular patches simultaneously from the onset to disappearance over the southern part of China and adjacent regions. The paper is arranged as follows: "Data and method" describes the data and method to obtain the keograms. The observation results are presented in "Results based on the ROTI

Fig. 1 Distribution of the GNSS receivers from CMONOC
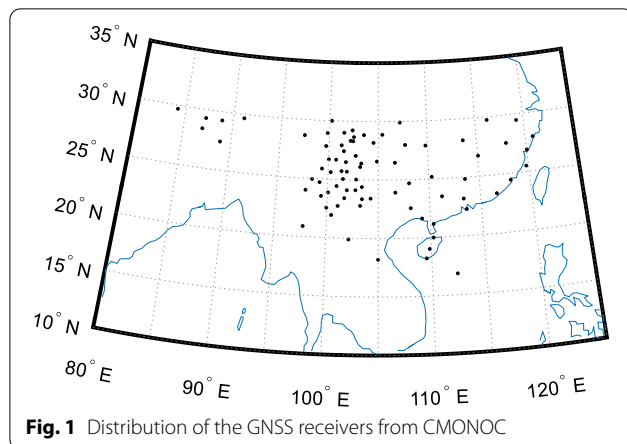
keograms in 2014", the discussion is presented in "Discussion", and "Summary" summarizes this work.

Data and method

Data and method to obtain the vertical ROTI

In this paper, 80 GNSS receivers of CMONOC at latitudes below 30 °N were used to study the ionospheric irregularities, as shown in Fig. 1. The black dots are the locations of the receivers. The spacing of the GNSS stations ranges from 38 to 885 km with an average of 232 km. The dashed lines showed the magnetic latitudes labeled on the right hand side axis. The distribution of GNSS receivers covers a longitudinal range of 40 degrees (zonal distance of ~4000 km) from ~85 to 125 °E. The selected receiver distribution is capable of continuously observing the temporal–spatial evolution of ionospheric irregularities in a large longitude range.

Based on the carrier phase measurements of the GNSS receivers, the slant TEC (sTEC) was calculated every 30 s for each receiver–satellite pair (Ma and Maruyama 2003). To mitigate multipath effects, only data with satellite elevation larger than 30 degrees were used. Rate of TEC (ROT) was determined by taking the difference between the sTECs at two consecutive times. ROTI is defined as the standard deviation of ROT in 5 min and it is used to quantify TEC fluctuation (Pi et al. 1997). ROTI is a measurement of the irregularities with scale-size in the order of tens of kilometers. To mitigate the effect of the elevation on ROTI, vROTI is calculated by vROTI = ROTI · cos χ. Here χ is the zenith angle of the satellite relative to vertical direction at ionospheric piercing point (IPP). The ionosphere is assumed to be a thin layer located at 400 km above the ground. For one GNSS receiver, an irregularity encounter is reckoned if more than 20 consecutive vROTIs are larger than a threshold. The threshold was determined by the following expression (Ma et al. 2019).

$$\text{vROTI}_{thrshld} = \text{vROTI}_{median} + 10 \times \text{vROTI}_{RMS}$$

Considering that the equatorial ionospheric irregularities usually occurred at night, vROTIs in the above expression (for calculating threshold) are collected during daytime 6:00 LT to 18:00 LT when vROTI is quiet. The threshold of vROTIs could be different for different receivers and was around 0.2 TECU/min.

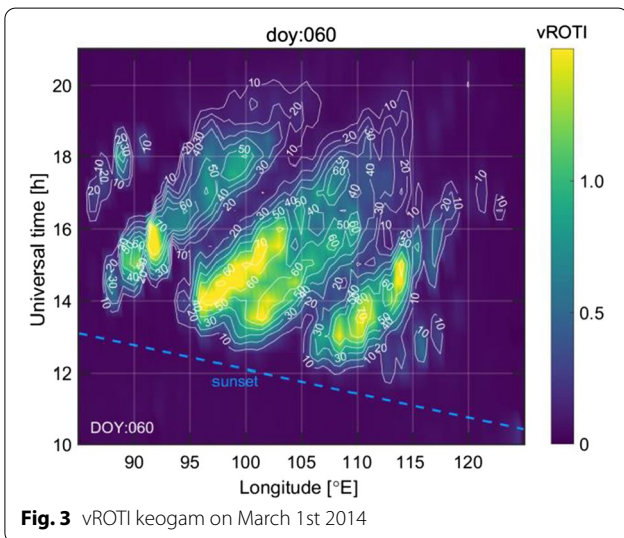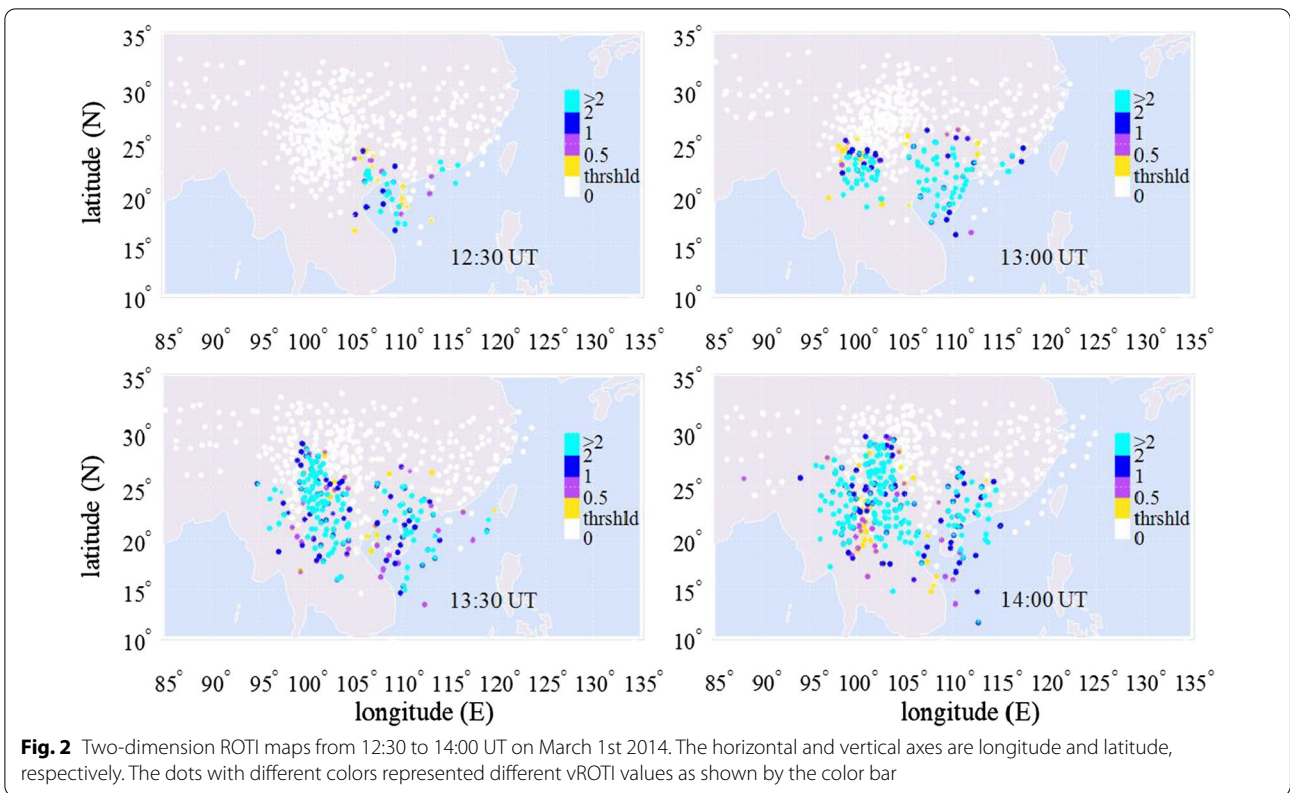### Method to obtain the longitude-time ROTI keogram

After vROTI was calculated for each IPP, two-dimension ROTI maps can be obtained to detect the ionospheric irregularities. Figure 2 shows four ROTI maps in a sequence from 12:30 to 14:00 UT on March 1st, 2014. The color bar showed vROTI values in TECU/min. The irregularities occurred at the east of 105 °E at 12:30. At 13:00 UT, another irregular patch appeared around 100 °E. The irregularities developed rapidly with time as can be seen at 13:30 and 14:00 UT.

For a better overview of the characteristics of the ionospheric irregularities, the longitude-time ROTI keograms are constructed as follows:

(a) Pick up all the vROTIs between 10:00 and 22:00 UT (18:00–06:00 Beijing Standard Time).
(b) Bin vROTIs according to the longitude and time, the longitude-time pixel is 0.5° × 30 min.
(c) Calculate the mean of vROTIs in each pixel.
(d) Calculate the percentage of vROTIs exceeding the threshold in each pixel.
(e) Construct vROTI keogram using the mean of vROTI in each pixel.
(f) Draw the contour line of the percentage of vROTIs exceeding the threshold in each pixel.

As a result of the construction of vROTI keogram, the latitudes are compressed. Figure 3 shows an example of the keogram on March 1st 2014. The horizontal axis is the longitude, and the vertical axis is the universal time. The color map represents the mean of vROTIs as indicated by the color bar on the right, and the white contours are the percentage of vROTIs exceeding the threshold. The blue dashed line indicates the E-region sunset time at 20 °N. Here 20 °N is chosen in view of (1) it is in the southern part of our observation, (2) the ionospheric irregularities mainly occurred at the magnetic equator and low latitudes. The sunset at 30 °N is ~6 min earlier than that at 20 °N. We consider 6 min to be an acceptable error for the 30 min resolution on the keogram.

Figure 3 reveals that the irregularities mainly appeared after E-region sunset. Four major patches can be clearly observed with an apparent longitudinal/zonal width of ~5 degrees. The real longitudinal width may be smaller

Fig. 2 Two-dimension ROTI maps from 12:30 to 14:00 UT on March 1st 2014. The horizontal and vertical axes are longitude and latitude, respectively. The dots with different colors represented different vROTI values as shown by the color bar

Fig. 3 vROTI keogam on March 1st 2014

than the apparent width, because the inclined patches of irregularity in real space and the latitude compression yield a large width of patches on the keogram.

The four major patches had a lifetime of 5~7 h. All of them did not stay at the same longitude but drifted eastward. For example the patch at 95 °E appeared at ~13:00UT. As time progressed, it arrived at 103 °E at ~16:00UT. This suggested that the patch of the irregularities moved eastward. The average eastward velocity can be estimated by the slope of the patch. It is difficult to obtain the variation of the velocity, because the keogram blends irregularities drifted from other longitude with the freshly generated irregularity. The average velocity is about 103 m/s assuming that the irregularities are at 20 °N. If the irregular patch is located at 15 °N or 25 °N, the velocity estimation will be ~106 m/s or ~100 m/s. Considering that the ionospheric irregularities usually appeared at the low latitude in the equinoxes, the irregularities are assumed to be at 20 °N in the speed estimation. The four major patches have similar slope, implying that they drifted eastward at similar speed. It can also be noted that vROTI along each patch gradually weakened over time until the patch finally disappeared.

It can also be noted that there are some meso-scale patches (zonal width of ~1−2 degrees/100−200 km) inside each large patch (zonal width of ~5 degrees). Owing to the pixel size of $0.5° \times 30$ min, irregular patches or structures smaller than ~100 km/~1 degree are obscured on the keograms. The irregularities in March, June,
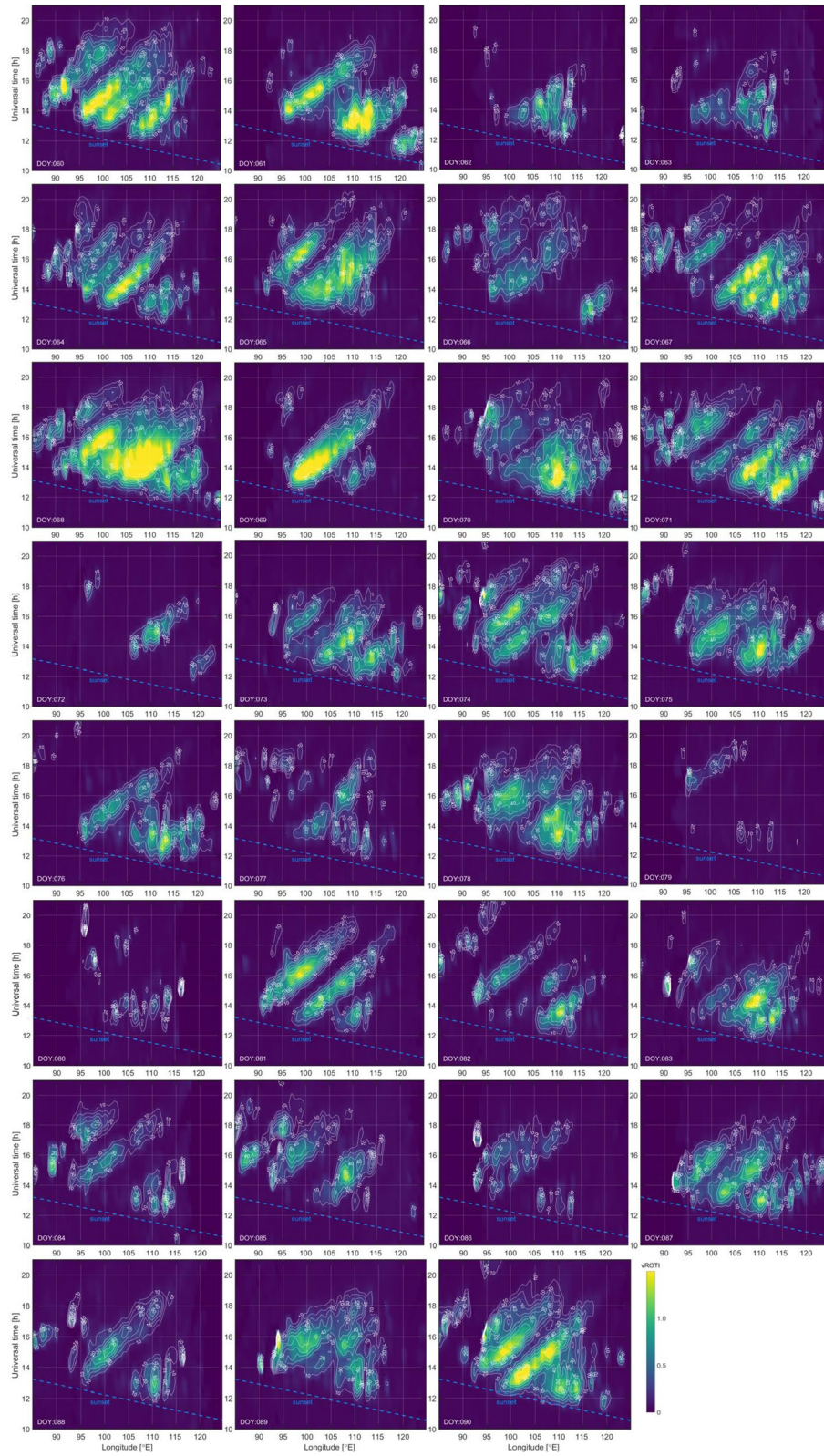
Fig. 4 vROTI keograms based on CMONOC in March 2014

Li *et al. Earth, Planets and Space*   (2022) 74:149

Page 6 of 12

September and December are analyzed in the following sections using the keograms based on CMONOC.

Results based on the ROTI keograms in 2014

Irregularities in March 2014

The ionospheric irregularities occurred every day in March 2014, as shown in Fig. 4. It can be seen that the irregularities had different characteristics day by day in this month. Most of time, the irregularities had several patches between 85 °E and 125 °E. They started to appear successively from east to west owing to different sunset time. In terms of the local time (LT), all of them appeared at ~ 19:00 LT. On most days the longitudinal width of the irregular patch is ~ 5 degree. However, the longitudinal gap between two neighboring patches generally varies. It can be noted that the longitudinal width of the patch is related to the strength of vROTI. The largest patch was

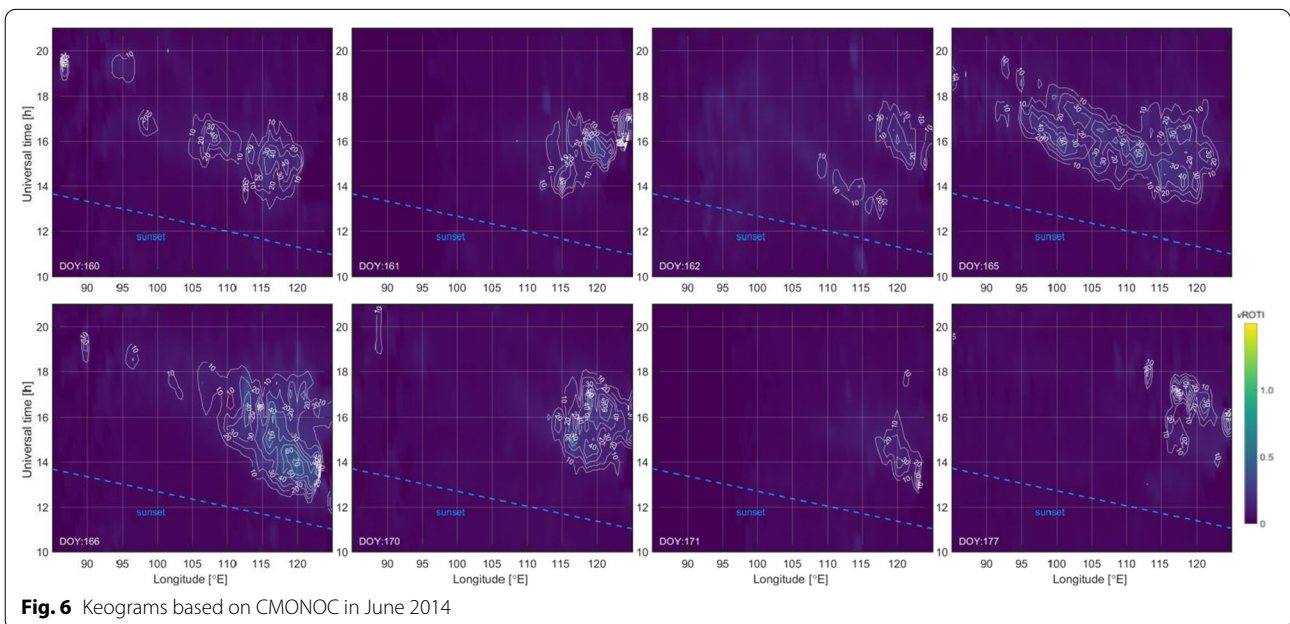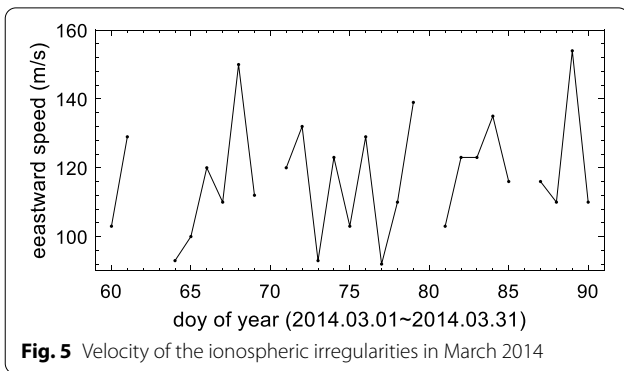**Fig. 5** Velocity of the ionospheric irregularities in March 2014

on the 68th day when vROTI was large, and the patches were smaller on the 79th and 80th day when vROTI was weak. Figure 4 also shows that there are some smaller patches within a large patch. For example, the west patch on the 61st day included three small patches with large vROTI.

On most days in March, the irregular patches on the keograms drifted eastward as time progressed. A clear eastward drift was usually observed for the cases of ionospheric irregularities with long lifetime (more than 4 h) and large vROTI values. On some days, the patches of irregularities did not show clear eastward drift, for example on the 62nd, 63rd, 77th, 79th, 80th and 86th days of the year 2014. On the aforementioned days, these irregularities had short lifetime, small longitudinal width and weak vROTI.

For the irregularities with clear eastward drift, the average velocity can be estimated from the vROTI keograms. The results of the average velocity estimation are shown in Fig. 5. The gaps in this figure correspond to cases with no clear eastward velocity from the keograms. The typical eastward velocity was about 120 m/s, with a range from 90 to 160 m/s.

Irregularities in June 2014

Figure 6 shows the vROTI keograms in June 2014. Ionospheric irregularities were encountered by CMONOC on 8 days in June (the monthly occurrence was 27%). The irregularities started to appear about 2–3 h after 19:00 LT. The irregularities did not drift eastward; but rather they often showed a westward drift in the summer
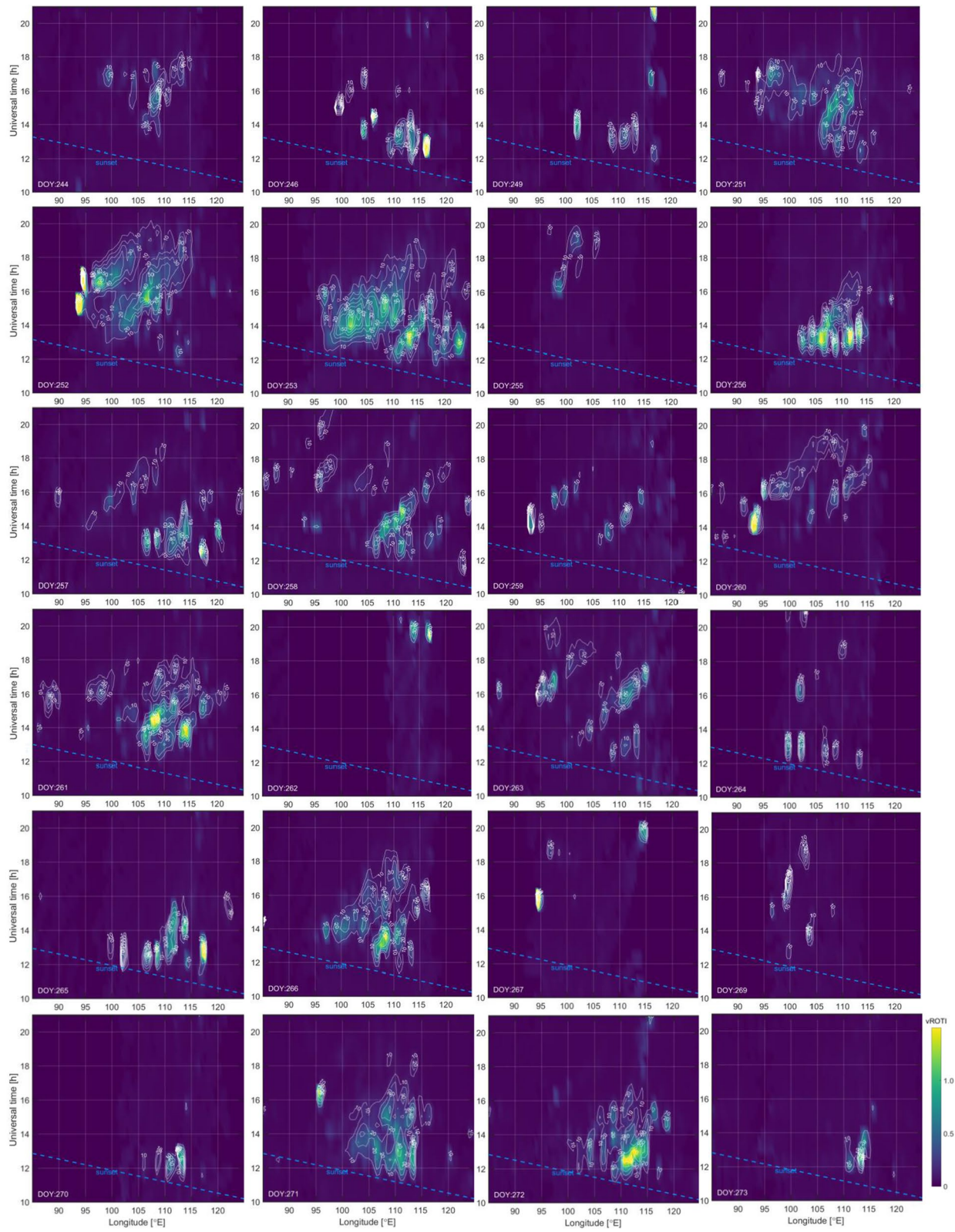

Fig. 6 Keograms based on CMONOC in June 2014

Li *et al. Earth, Planets and Space* (2022) 74:149

Page 7 of 12

Fig. 7 Keograms from CMONOC in September 2014

Li *et al. Earth, Planets and Space*   (2022) 74:149

Page 8 of 12

solstice month. The average westward velocity was about 80–130 m/s. The lifetime of the irregularities was about 3–6 h. Compared with those in March, the irregularities in June had weaker vROTI and shorter lifetime.

Irregularities in September 2014

In September, the irregularities observed on the vROTI keograms are shown in Fig. 7. There were 24 days on which the irregularities occurred. The monthly occurrence rate of 80% was higher than the occurrence rate in June and lower than that in March. The start time of the irregularities was often at 19:00 LT. In September the irregularities had large spatiotemporal extent only on several days. The large patches also drifted eastward

like those in March. Most of the time the irregularities in our observation range consisted of several small patches. Every patch had a lifetime of ~1 h and longitudinal width of ~2 degrees. These small patches did not show clear drift on the vROTI keograms. The strength of vROTI in September was stronger than that in June but weaker than that in March.

Irregularities in December 2014

In December, the irregularities appeared on 15 days which correspond to a monthly occurrence rate of 48%. The irregularities in this month were very different from other 3 months. The keograms are shown in Fig. 8. The patches were discrete/localized with short lifetime. On
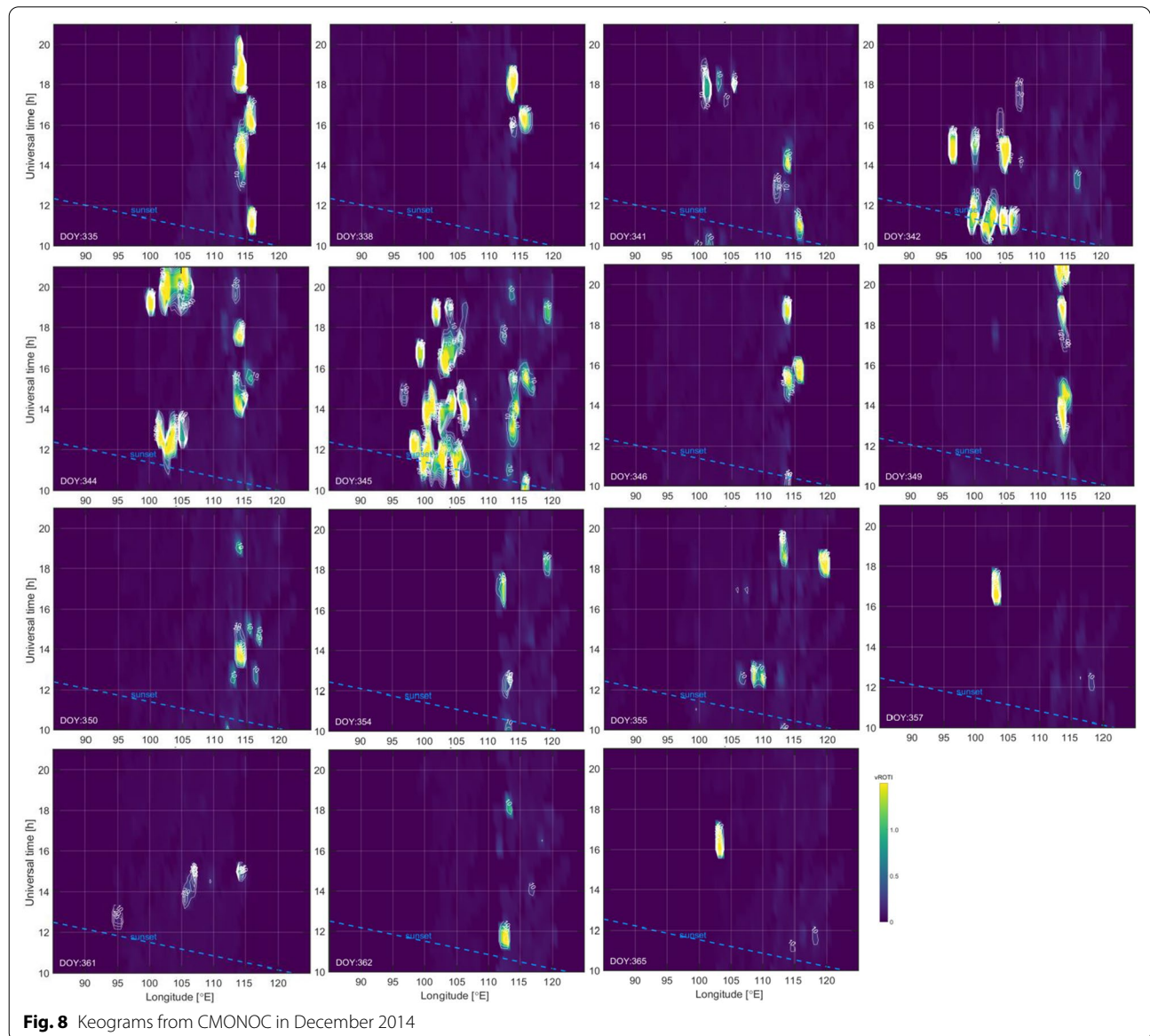

Fig. 8 Keograms from CMONOC in December 2014

Li *et al. Earth, Planets and Space*   (2022) 74:149

Page 9 of 12

the 335th day, the irregularities continued sporadically from 10:00 to 20:00 UT at the longitude of 115 °E. On the 345th day, the irregularities appeared discretely in a large longitude and time range. In addition, on the 357th and 365th days, only one irregular patch was observed. Although the patches of irregularities appeared at different time and longitude range, all the patches had similar longitudinal width of ~2 degrees and lifetime of about 1–2 h. The patches of irregularities on the same day were discrete in time and longitude. They may not be associated with each other. It should also be noted that the irregularities in December had stronger vROTI than those in June and September, and they did not drift eastward or westward on the keograms.

Discussion

The keograms based on CMONOC in 2014 showed that the irregularities had the highest monthly occurrence rate in March of almost 100%, then 80% in September, 48% in December and 27% in June. The high occurrence in both equinoxes and low occurrence in two solstices are consistent with previous results (Su et al [2008]; Thanh et al. [2021]). The seasonal characteristics of occurrence rate showed good correspondence with the vertical drift velocities of the ionospheric plasma (Vyas and Dayanandan [2011]; Su et al. [2008]).

The longitudinal/zonal width of the patches is ~5° in March, larger than the zonal width of the striations observed by Buhari et al. ([2014]), Diego Barros et al. ([2018]) and de Jesus et al. ([2020]). The large width may be owing to the large distance of our receivers and the latitude compression on the keograms. Longitudinal width of ~5° has also been detected by Defense Meteorological Satellite Program (DMSP) spacecraft in the longitude of 110–120 °E (Burke et al. [2004]). It should also be mentioned that the patches separated longitudinally. Patra et al. ([2016]) suggested that the longitudinally localized plasma irregularities are linked with the magnetic storm-related electric field in the dusk sector and a complex interplay of prompt penetration and disturbance dynamo electric fields during the later part in the night. However, in this work, the geomagnetic field is quiet on most of days. Further investigation is required to understand the longitudinally localized irregularities on the geomagnetic quiet days.

The keograms in March showed that the irregularities had long lifetime. They usually lasted several hours or till early morning. The latitude information of the irregularities was lost on the longitude-time ROTI keograms. To understand the latitude information of the irregularities, the latitude ranges of the irregularities based on the latitude-time keograms are summarized in Fig. 9. It can be seen that in March the irregularities extended from
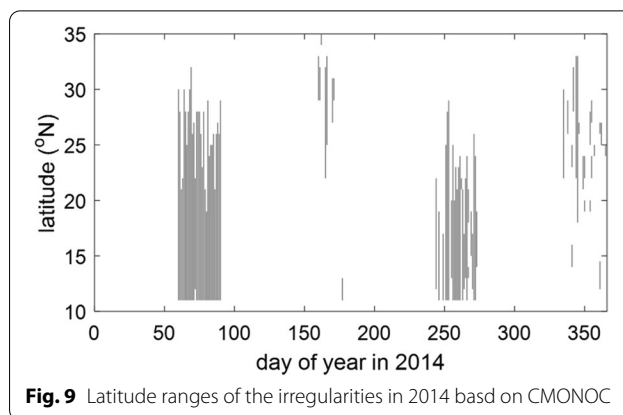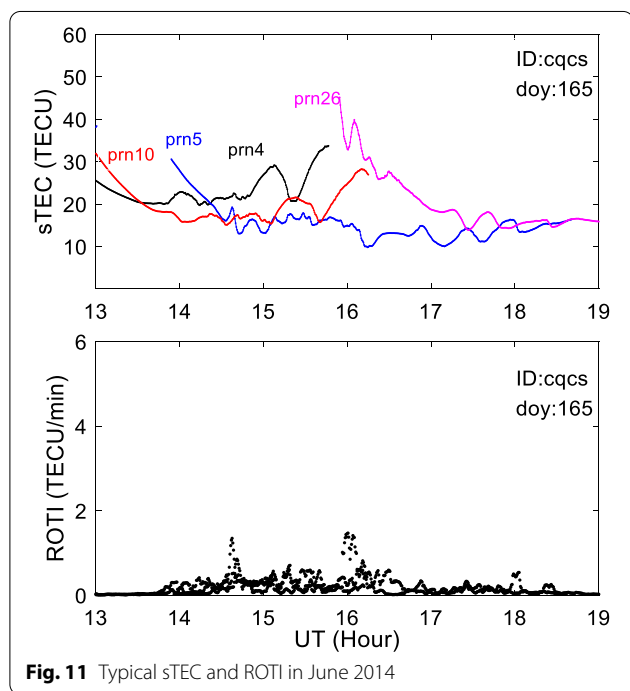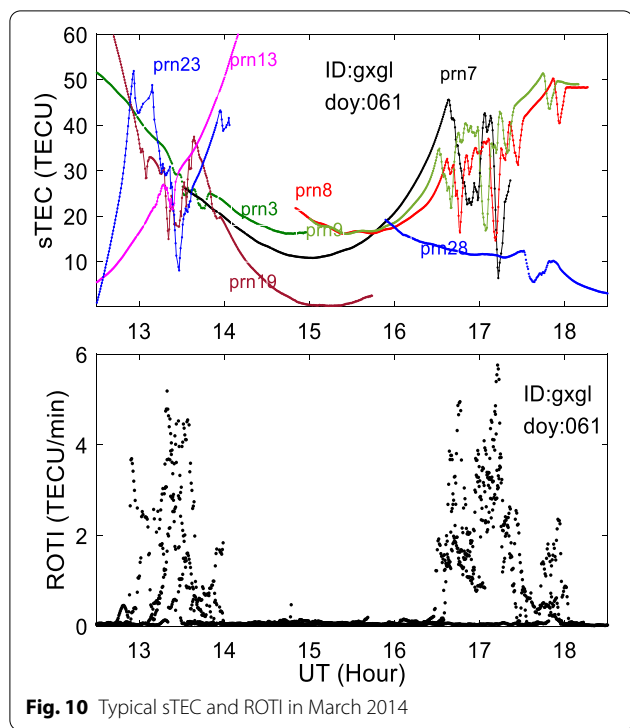

Fig. 9 Latitude ranges of the irregularities in 2014 basd on CMONOC

11 °N to 30 °N (magnetic latitude: ~4–26 °N). It should be noted that the irregularities did not extend beyond 23 °N on the 62nd, 63rd, 72nd, 77th, 79th, 80th and 86th days of year, on which the irregularities had short lifetime, small longitudinal width and weak vROTI. The long lifetime patches and strong ROTI should be associated to the location of equatorial ionization anomaly (EIA) crest. Macho et al. ([2022]) pointed that during 2012–2015 scintillation the EIA crest centered 20–30 °N, where the scintillation activity was intense. Chandra et al. ([1993]) showed that VHF scintillations at the station close to the magnetic equator were strong and lasted till early morning in single patch during March–April 1991 in India. The long lifetime and large spatial size of patches observed in March 2014 are in agreement with the observation by Chandra et al. ([1993]). Chandra et al ([1993]) also pointed that VHF scintillations occurred in small patches with periods of no scintillations in between for the station in the anomaly crest region or beyond. However, from the keograms in March there were few small patches discrete in time although our observation range covered the anomaly crest region. This difference may be due to two reasons; one is that VHF scintillation is sensitive to irregularities with spatial length of hundreds of meters, while ROTI keogram with the pixel of 0.5° × 30 min obscured the patches smaller than ~100 km; the other is that ROTI keograms compressed the latitude information so that the difference with latitudes cannot be detected. Figure 10 shows the typical sTEC and ROTI in March 2014. Here sTEC minus some fixed values are presented to show the relative variation in the same scale. In the study of ionospheric irregularities, what matters the most is the relative changes that occur. From Fig. 10, it can be seen that the sTEC suddenly dropped when the satellite encountered an ionospheric irregularity. This feature is the typical characteristic of the EPBs.

The average eastward velocity was ~90–160 m/s. Previous results also showed that the typical eastward drift

Li *et al. Earth, Planets and Space*   (2022) 74:149

Page 10 of 12

Fig. 10 Typical sTEC and ROTI in March 2014

Fig. 11 Typical sTEC and ROTI in June 2014

velocity of the ionospheric irregularities is on the order of ~ 100–200 m/s (Valladares et al. 1996;). Chapagain et al. (2012) pointed that the observed ionospheric

irregularities velocity is consistent with the ambient plasma, which drifts eastward at nighttime (Fejer et al. 1991).

In June, the large patches of the irregularities had a westward drift at a speed of 80–130 m/s. This was different from the EPBs. Figure 11 presents the typical sTEC and ROTI in June. It can be noted that the irregularities described by ROTI do not always match with the sTEC undulation (wave-like perturbation). Only rapid undulation of sTEC caused large ROTI. Unlike the irregularities with a sharp drop of sTEC in March, the irregularities in June are related to the rapid sTEC undulation. Figure 9 shows that the irregularities in June often appeared at ~ 30 °N. The irregularities in June with westward drift may be related to the medium-scale traveling ionospheric disturbances (MSTIDs). In addition, the sTEC undulation is similar to the pattern of MSTIDs. Previous studies pointed that the nighttime MSTIDs are mainly observed in middle latitude and their propagation direction is primarily southwestward in the northern hemisphere (Otsuka et al. 2004; Takahashi et al. 2018). They are more active during June solstice and they can propagate to lower latitude (Sivakandan et al. 2019).

In September, the occurrence rate, the lifetime, the ROTI values and the longitudinal width of the patches were lower/shorter/weaker/smaller than those in March. The occurrence time and the eastward drift were similar to those in March, and different from those in solstice months. Previous study also showed the equinoctial asymmetry in the occurrence, which was greater in the spring equinox than in the autumn equinox (Nishioka et al. 2008; Maruyama et al. 2009; Otsuka et al. 2006; Sripathi et al. 2011). The asymmetry may be attributed to differences in plasma densities and meridional winds during the two equinoxes (Nishioka et al. 2008; Maruyama et al. 2009; Otsuka et al. 2006; Sripathi et al. 2011).

In China, the irregularities are rarely reported in December. The GPS scintillation at Guangzhou (113.34 °E, 23.16 °N) and Shenzhen (113.97 °E, 22.59 °N) occurred mainly in the equinox months. In enhanced solar activity years, the occurrence increased not only in the equinox months but also in summer and winter (Deng et al. 2013). In this work, the observations are from 2014, a maximum solar activity year. The occurrence reached 27% and 48% in June and December, respectively, in the range of 85–125 °E. Higher latitude observations range (IPPs covering 11–35 °N) in this work should contribute to the occurrence of the irregularities in summer and winter. Figure 9 shows that the summer/winter irregularities mainly appeared at 20–30 °N.

The higher occurrence in winter than in summer is rarely reported in Southeast Asia (Li et al. 2021). Thanh

Li *et al. Earth, Planets and Space*   (2022) 74:149

Page 11 of 12

et al. (2021) studied the occurrence rate of the irregularities by ROTI over Southeast Asian region from 2008 to 2018. Their results for 2014 showed that only at CUSV (13.74 °N, 100.53 °E) station the occurrence rate in December is higher than that in June. At MTEV (22.39 °N, 102.81 °E) and SMAV (21.06 °N, 103.75 °E), the occurrence in June are larger than that in December (Thanh et al. 2021). Some researchers found that the occurrence rate of VHF scintillation or spread F in the low-latitude of Indian sector peaked in the equinoxes and winter during the high solar activity period; and during the low solar activity period the occurrence peaked in equinoxes and summer (Sushil and Gwal 2000; Singh et al. 2004; Vyas and Dayanandan 2011; Sahithi et al. 2019; Raghunath and Ratnam 2015). The higher occurrence rate in winter than that in summer is consistent with the results in Indian sector, but it is different from those over Southeast Asian region. From the keograms, it can be seen that the irregularities in December is patchy and discrete/localized. Vyas and Dayanandan (2011) pointed that patchy and discrete are the features of scintillations over equatorial anomaly region. The patchy and discrete irregularities can cause different occurrence rate at different stations. At some stations the occurrence rate in summer is higher than that in winter. At others, the occurrence rate in winter is higher. However, within our whole observation range the occurrence rate in winter is higher than that in summer.

Summary

Dual-frequency GPS observations from CMONOC were used to analyze the irregularities in 2014 over the south of China. The longitude-time vROTI keograms were obtained by binning the observations into $0.5° \times 30$ min longitude-time grid cells. The irregularities usually included several patches on our observation range. The longitudinal width, the lifetime and the average velocity of each patch can be estimated from the keograms. The results showed that the ionospheric irregularities had the highest occurrence rate of 100% in March, then in September, December and the lowest in June. In March the irregularities had an apparent longitudinal scale of ~5 degree and most of the time they drift eastward at an average velocity of ~100 m/s with a long lifetime of 5–7 h. Sometimes, the irregularities just stayed at the same longitude, with weak ROTI and short lifetime. The irregularities in September are similar to those in March except weaker ROTI and shorter lifetime. In the solstice months, the irregularities appeared at higher latitudes than those in equinoxes. They had different characteristics in the two solstice months. In June, the irregularities usually had weak ROTI and drifted westward. However, in December they were patchy and discrete with stronger ROTI than those in June and September. The irregularities in the equinox months should be from lower latitudes beyond our observations. The irregularities in the solstice months may be local phenomena, intrinsic to the midlatitude region and unrelated to extension of EPBs from low-latitude regions within the same longitude sector. Further studies are needed to understand the features of the irregularities in June and December.

Declarations

Author details
[1]National Astronomical Observatories Chinese Academy of Sciences, Beijing, China. [2]University of Chinese Academy of Sciences, Beijing, China. [3]National Institute of Information and Communications Technology, Tokyo, Japan.

References
Aa E, Huang W, Liu S, Ridley A, Zou S, Shi L, Chen Y, Shen H, Yuan T, Li J, Wang T (2018) Midlatitude plasma bubbles over China and adjacent areas during a magnetic storm on 8 September 2017. Space Weather 16:321–331. https://doi.org/10.1002/2017SW001776

Li *et al. Earth, Planets and Space*   (2022) 74:149

Page 12 of 12

Barros D, Takahashi H, Wrasse CM, Cosme AO, Figueiredo B (2018) Characteristics of equatorial plasma bubbles observed by TEC map based on ground-based GNSS receivers over South America. Ann Geophys 36:91–100. https://doi.org/10.5194/angeo-36-91-2018

Buhari SM, Abdullah M, Hasbi AM, Otsuka Y, Yokoyama T, Nishioka M, Tsugawa T (2014) Continuous generation and two-dimensional structure of equatorial plasma bubbles observed by high-density GPS receivers in Southeast Asia. J Geophys Res Space Physics 119:10569–10580. https://doi.org/10.1002/2014JA020433

Burke WJ, Gentile LC, Huang CY, Valladares CE, Su SY (2004) Longitudinal variability of equatorial plasma bubbles observed by DMSP and ROCSAT-1. J Geophys Res 109:A12301. https://doi.org/10.1029/2004JA010583

Chandra H, Vyas GD, Rao DRK, Pathan BM, Iype A, Ram SB, Naidu A, Sadique SM, Salgaonkar CS, Tyagi TR, Vijay KPN, Lakha S, Iyer KN, Pathak KN, Gwal AK, Sushil K, Singh RP, Singh UP, Birbal S, Jain VK, Navneeth GN, Koparkar PV, Rama RPVS, Jaychandran PT, Sriram P, Santa RNYS, Das GA, Basu K, Rastogi RG (1993) Coordinated multistation VHF scintillation observations in India during March–April 1991. Indian J Radio Space Phys 22:69–81

Chapagain NP, Taylor MJ, Makela JJ, Duly TM (2012) Equatorial plasma bubble zonal velocity using 630.0 nm airglow observations and plasma drift modeling over Ascension Island. J Geophys Res 117:A06316. https://doi.org/10.1029/2012JA017750

Cherniak IV, Krankowski A, Zakharenkova I (2018) ROTI Maps, a new IGS ionospheric product characterizing the ionospheric irregularities occurrence. GPS Solut. https://doi.org/10.1007/s10291-018-0730-1

de Jesus R, Batista IS, Takahashi H, de Paula ER, Barros D, Figueiredo CAOB et al (2020) Morphological features of ionospheric scintillations during high solar activity using GPS observations over the South American sector. J Geophys Res Space Phys. https://doi.org/10.1029/2019JA027441

Deng B, Huang J, Liu W, Xu J, Huang L (2013) GPS scintillation and TEC depletion near the northern crest of equatorial anomaly over South China. Adv Space Res 51(3):356–365

Fejer BG, de Paula ER, Gonzilez SA, Woodman RF (1991) Average vertical and zonal F region plasma drift over Jicamarca. J Geophys Res 96(A8):13901–13906

Hernández-Pajares M, Juan JM, Sanz J, Orus R, Garcia-Rigo A, Feltens J, Komjathy A, Schaer SC, Krankowski A (2009) The IGS VTEC maps: a reliable source of ionospheric information since 1998. J Geod 83:263–275. https://doi.org/10.1007/s00190-008-0266-1

Kintner P, Ledvina B, de Paula E, Kantor I (2004) Size, shape, orientation, speed, and duration of GPS equatorial anomaly scintillations. Radio Sci 39(2):RS2012

Li G, Ning B, Otsuka Y, Abdu MA, Abadi P, Liu Z, Spogli L, Wan W (2021) Challenges to equatorial plasma bubble and ionospheric scintillation short-term forecasting and future aspects in east and southeast Asia. Surv Geophys 42:201–238. https://doi.org/10.1007/s10712-020-09613-5

Ma G, Maruyama T (2003) Derivation of TEC and estimation of instrumental biases from GEONET in Japan. Ann Geophys 21(10):2083–2093

Ma G, Hocke K, Li J, Wan Q, Lu W, Fu W (2019) GNSS ionosphere sounding of equatorial plasma bubbles. Atmosphere 10:676. https://doi.org/10.3390/atmos10110676

Macho EP, Correia E, Spogli L, Muella M (2022) Climatology of ionospheric amplitude scintillation on GNSS signals at south American sector during solar cycle 24. J Atmos Solar Terr Phys 231:105872

Maruyama T, Saito S, Kawamura M, Nozaki K, Krall J, Huba JD (2009) Equinoctial asymmetry of a low-latitude ionosphere-thermosphere system and equatorial irregularities: evidence for meridional wind control. Ann Geophys 27:2027–2034

Nishioka M, Saito A, Tsugawa T (2008) Occurrence characteristics of plasma bubble derived from global ground-based GPS receiver networks. J Geophys Res 113:A05301

Otsuka Y, Shiokawa K, Ogawa T, Yokoyama T, Yamamoto M, Fukao S (2004) Spatial relationship of equatorial plasma bubbles and field-aligned irregularities observed with an all-sky airglow imager and the Equatorial Atmosphere Radar. Geophys Res Lett 31(20):L20802

Otsuka Y, Shiokawa K, Ogawa T (2006) Equatorial ionospheric scintillations and zonal irregularity drifts observed with closely-spaced GPS receivers in Indonesia. J Meteorol Soc Jpn 84A:343–351

Patra AK, Chaitanya PP, Dashora N, Sivakandan M, Taori A (2016) Highly localized unique electrodynamics and plasma irregularities linked with the 17 March 2015 severe magnetic storm observed using multitechnique common-volume observations from Gadanki, India. J Geophys Res Space Phys 121:11518–11527. https://doi.org/10.1002/2016JA023384

Pi X, Mannucci AJ, Lindqwister UJ, Ho CM (1997) Monitoring of global ionospheric irregularities using the worldwide GPS network. Geophys Res Lett 24:2283–2286

Raghunath S, Ratnam DV (2015) Detection of low-latitude ionospheric irregularities from GNSS observation. IEEE J Sel Top Appl Earth Obs Remote Sens 8(11):5171–5176

Sahithi K, Sridhar M, Kotamraju SK, Kavya KCS, Sivavaraprasad G, Ratnam DV, Deepthi C (2019) Characteristics of ionospheric scintillation climatology over Indian low-latitude region during the 24th solar maximum period. Geod Geodyn 10(2):110–117. https://doi.org/10.1016/J.GEOG.2018.11.006

Singh RP, Patel RP, Singh AK (2004) Effect of solar and magnetic activity on VHF scintillations near the equatorial anomaly crest. Ann Geophys 22:2849–2860. https://doi.org/10.5194/angeo-22-2849-2004

Sivakandan M, Chakrabarty D, Ramkumar TK, Guharay A, Taori A, Parihar N (2019) Evidence for deep ingression of the midlatitude MSTID into as low as ~3.5° magnetic latitude. J Geophys Res: Space Phys 124:749–764. https://doi.org/10.1029/2018JA026103

Sripathi S, Kakad B, Bhattacharyya A (2011) Study of equinoctial asymmetry in the Equatorial Spread F (ESF) irregularities over Indian region using multi-instrument observations in the descending phase of solar cycle 23. J Geophys Res 116:A11302. https://doi.org/10.1029/2011JA016625

Su S-Y, Chao CK, Liu CH (2008) On monthly/seasonal/longitudinal variations of equatorial irregularity occurrences and their relationship with the post sunset vertical drift velocities. J Geophys Res 113:A05307. https://doi.org/10.1029/2007JA012809

Sushil K, Gwal AK (2000) VHF ionospheric scintillations near the equatorial anomaly crest: solar and magnetic activity effects. J Atmos Solar Terr Phys 62:157–167

Takahashi H, Wrasse CM, Figueiredo C, Barros D, Abdu MA, Otsuka Y, Shiokawa K (2018) Equatorial plasma bubble seeding by MSTIDs in the ionosphere. Prog Earth Planet Sci 5:32. https://doi.org/10.1186/s40645-018-0189-2

Thanh DN, Le Huy M, Amory-Mazaudier C, Fleury R, Saito S et al (2021) Characterization of ionospheric irregularities over Vietnam and adjacent region for the 2008–2018 period. Vietnam J Earth Sci, Vietnam Acad Sci Technol. https://doi.org/10.15625/2615-9783/16502

Valladares CE, Sheehan R, Basu S, Kuenzler H, Espinoza J (1996) The multi-instrumented studies of equatorial thermosphere aeronomy scintillation system: climatology of zonal drifts. J Geophys Res 101:26839–26850

Vyas BM, Dayanandan B (2011) Nighttime VHF ionospheric scintillation characteristics near the crest of Appleton anomaly station Udaipur (24.6°N, 73.7°E). Indian J Radio Space Phys 40:191

Wei G, Huang W, Liu G, Aa E, Liu S, Chen Y, Luo B (2020) Generation of ionospheric scintillation maps over Southern China based on Kriging method. Adv Space Res 65(12):2808–2820

Publisher's Note